ChemPubSoc Europe

DOI: 10.1002/chem.201900136

CHEMISTRY A European Journal Full Paper

Fluorophores

Intramolecular Phosphacyclization: Polyaromatic Phosphonium P-Heterocycles with Wide-Tuning Optical Properties

Andrey Belyaev,[a] Yi-Ting Chen,[b] Zong-Ying Liu,[b] Philip Hindenberg,[c] Cheng-Ham Wu,[b] Pi-Tai Chou,*[b] Carlos Romero-Nieto,*[c, d] and Igor O. Koshevoy*[a]

Abstract: Rationally designed cationic phospha-polyaromatic fluorophores were prepared through intramolecular cyclization of the tertiary *ortho*-(acene)phenylene-phosphines mediated by Cu^{II} triflate. As a result of phosphorus quaternization, heterocyclic phosphonium salts **1c**–**3c**, derived from naphthalene, phenanthrene, and anthracene cores, exhibited very intense blue to green fluorescence ($\Phi_{em} = 0.38$–0.99) and high photostability in aqueous medium. The structure–emission relationship was further investigated by tailoring the electron-donating functions to the anthracene moiety to give dyes **4c**–**6c** with charge-transfer character. The latter significantly decreases the emission energy to reach near-IR region. Thus, the intramolecular phosphacyclization renders an ultra-wide tuning of fluorescence from 420 nm (**1c**) to 780 nm (**6c**) in solution, extended to 825 nm for **6c** in the solid state with quantum efficiency of approximately 0.07. The physical behavior of these new dyes was studied spectroscopically, crystallographically, and electrochemically, whereas computational analysis was used to correlate the experimental data with molecular electronic structures. The excellent stability, water solubility, and attractive photophysical characteristics make these phosphonium heterocycles powerful tools in cell imaging.

Introduction

Rational design and tailoring of the properties of molecular luminophores is a key element that eventually determines the progress in a number of practically important fields including organic electronics,[1] optical sensing[2] and fluorescence imaging.[2a,3] The growing needs for efficient light-emitting compounds with specific functionalities necessarily require judicious design of new chromophore blocks. The latter, in turn, implies the development of new synthetic strategies and establishing the relationships between the molecular structure and physical characteristics. As has been highlighted in the series of recent reviews, fusion of the π-conjugated motifs with heterocyclic fragments, incorporating 3p elements and particularly those containing phosphorus,[4] produces extended systems with unique electronic properties and, consequently, intriguing optical behavior.

Thanks to the accessible formation of the tertiary $\lambda^3\sigma^3$ phosphorus configuration, a wide range of organophosphorus molecular materials have been reported up to date, which can be embedded in diverse carbon-rich aromatic environments and can undergo facile transformation into the $\lambda^5\sigma^4$ derivatives through oxidation (to give the P-oxides/sulfides) or into the $\lambda^4\sigma^4$ analogues by reaction with metal complexes and other Lewis acids or quaternization (leading to ionic phosphonium cations). These versatile chemical modifications potentially provide broad possibilities to modulate the photophysical and electrochemical properties of the target compounds. As a matter of fact, the pronounced electron-withdrawing nature of the $\lambda^5\sigma^4$ and $\lambda^4\sigma^4$ phosphorus centers may offer additional ways to influence the energetics and localization of frontier molecular orbitals (primarily highest occupied MO and lowest unoccupied MO), which, importantly, must rely on the decoration of the chromophore core with electron-rich groups to afford push–pull (donor–acceptor) architectures with variable HOMO–LUMO gap.

Within the framework of the given general methodology, extensive studies were devoted to the family of dyes based on the five-membered phospholes.[5] The prominent feature of these heterocycles, especially those containing a pentavalent P

[a] *A. Belyaev, Prof. I. O. Koshevoy*
Department of Chemistry, University of Eastern Finland
Yliopistokatu 7, 80101 Joensuu (Finland)
E-mail: igor.koshevoy@uef.fi

[b] *Y.-T. Chen, Z.-Y. Liu, C.-H. Wu, P.-T. Chou*
Department of Chemistry, National (Taiwan) University, Taipei 106 (Taiwan)
E-mail: chop@ntu.edu.tw

[c] *P. Hindenberg, Dr. C. Romero-Nieto*
Organisch-Chemisches Institut, Ruprecht-Karls-Universität Heidelberg
Im Neuenheimer Feld 270, 69120 Heidelberg (Germany)
E-mail: carlos.romero.nieto@oci.uni-heidelberg.de

[d] *Dr. C. Romero-Nieto*
Faculty of Pharmacy, University of Castilla-La Mancha
Calle Almansa 14 - Edif. Bioincubadora, 02008, Albacete (Spain)

Supporting information and the ORCID identification number(s) for the author(s) of this article can be found under: https://doi.org/10.1002/chem.201900136.

atom, is a phenomenon of hyperconjugation. Such σ*(*exo*-P-C)-π* interaction markedly stabilizes the LUMO level and ensures the tunability of their electron-accepting properties. Notwithstanding, further reduction of the LUMO level may be achieved by the quaternization of the P atom affording the positively charged phosphonium salts. Thus, not surprisingly, the phosphole derivatives have been successfully employed in the fabrication of electroluminescent devices,[6] optical switches,[7] and sensors[8] in addition to light harvesting,[9] semiconducting,[10] and electrochromic materials.[11]

The chromophores constructed around six-membered phosphacycles have been lately recognized as an alternative avenue to the photoactive molecular materials.[4f,12] The larger size of the ring assumes richer opportunities for adjusting the electronic features and physicochemical functionality through more diverse structural variations of the heterocycle composition and the lateral substituents. The notable advancement of this class of compounds as fluorescent systems is associated with the phosphorus analogues of well-known dyes, such as rhodamine,[13] rhodol,[14] and fluorescein.[15] It is essential that these phospha-derivatives exhibit substantial bathochromic shift of absorption and emission reaching near-IR region along with high photostability in aqueous media that enabled their application in cell imaging.[16] A promising approach to the P-heterocyclic dyes covering a wide range of emission energies has been illustrated by the family of 2,6-dicyano-λ^5-phosphinines, the parent motif of which was obtained in high yield through a simple one-pot reaction.[17]

Nevertheless, the effective fusion of six-membered phosphacycles with extended conjugated (polyaromatic) fragments, which is anticipated to afford new and tunable chromophores, still represents a significant synthetic obstacle.[4d,18] One quite general preparative method of electrophilic intramolecular cyclization was discovered for naphthalene chlorophosphane precursors to give a series of neutral phosphaphenalene P-oxides.[19] The latter exhibited remarkable photophysical properties; they mostly emitted in the blue/green region of the visible spectrum and reached fluorescence quantum yields (Φ_{em}) up to 0.8. Remarkably, two different copper(II)-mediated phosphaannulation reactions, which lead to phosphonium salts, have been realized for the anthracene-based tertiary phosphanes.[20] Due to the cationic nature, these dyes showed good water solubility, retaining intense green-yellow fluorescence (536 nm) with Φ_{em} close to the unity in aqueous medium along with reasonable two-photon absorption ability. Taking into account their very low cytotoxicity, such fluorophores have a promising potential as intracellular imaging agents.[20b]

In view of these precedents, we envisaged the preparation of a new generation of improved organophosphorus dyes aiming to reach NIR luminescence. To that end, we attempted to keep control over the HOMO–LUMO gap in a series of fused six-membered phosphacycles by systematically varying the extension of their π-conjugation and utilizing a donor–acceptor approach; the latter implies the synergistic combination of the prominent electron-accepting capabilities of the quaternized P atoms and the careful decoration of fused six-membered phosphorus cores with electron-donating moieties. Thus, we report a successful strategy to control the optical band gap of originally blue-emitting six-membered phosphorus heterocycles to afford efficient NIR emitters suitable for bio-imaging applications.

Results and Discussion

Molecular design

The phosphorus-based scaffold, which we considered in our strategy for the preparation of dyes with wide alteration of emission energies, is shown in Figure 1. It consists of a fused

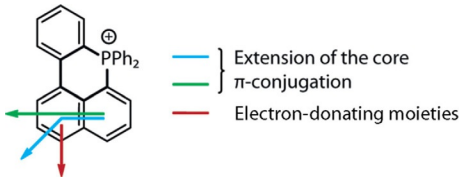

Figure 1. The proposed strategy to control the optical bandgap of positively charged fused six-membered phosphacycles.

six-membered phosphacycle containing a strong electron-accepting center; that is, a quaternized phosphorus atom with two phenyl groups. To reduce the optical band gap and access NIR luminescence, we explored structural modifications mainly focused on: 1) increasing the extension of the π-conjugation of the central polyaromatic core, and 2) decorating the main scaffold with electron-donor moieties (Figure 1).

Following this approach, we designed a series of synthetically accessible P heterocyclic molecules **1c**–**6c** (Figure 2, "**c**" indicates the cyclization product). Within this family, derivatives

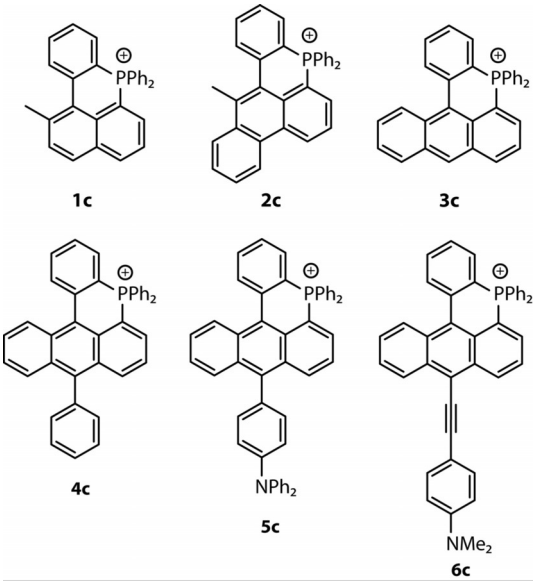

Figure 2. Designed fused six-membered phosphacycles to systematically tune the emission properties.

1c–**3c** differ by the degree of π-conjugation of the central core (naphthalene, phenanthrene and anthracene) and thus allow for the investigation of the impact of the polyaromatic framework on the optical behavior. In turn, cations **4c**–**6c** are modified with electron-donor functionalities of variable strength and the length of the connecting spacer. The latter, combined with the electron deficient nature of phosphonium group, affords efficient D–A systems capable of low energy intramolecular charge transfer, consequently reducing the optical bandgap.

Synthesis and characterization

The key synthetic step to generate six-membered heterocycles containing a positively charged phosphorus atom fused with polyaromatic systems involves an intramolecular ring closure that occurs in *ortho*-functionalized triphenylphosphines **1**–**6** in the presence of a stoichiometric amount of $Cu(OTf)_2$ salt (Scheme 1). Initially, the starting acenes (naphthalene, phenanthrene and anthracene)[21] were converted into iodo-substituted derivatives,[22] which were further transformed into *ortho*-bromophenyl intermediates by Suzuki cross-coupling reactions in good yields (69–71%, Scheme S1 in the Supporting Information). In addition, the 9-(2-bromophenyl)anthracene core was conventionally modified by bromination with *N*-bromosuccinimide at 10-position, followed by coupling with electron-donor groups to produce extended conjugated platforms for **5c** and **6c** species, as illustrated in Schemes 2 and S1 (Supporting Information).

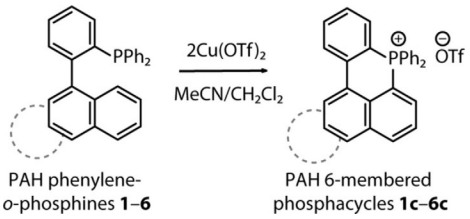

Scheme 1. Phosphaanulation reaction to attain P-heterocyclic dyes **1c**–**6c** (PAH = polycyclic aromatic hydrocarbon).

ortho-Phenylphosphines **1**–**6** were obtained through a standard protocol that includes lithiation of the bromoarene precursors and subsequent treatment with a stoichiometric amount of chlorodiphenylphosphane. These compounds were readily isolated as white (**1**–**3**) to yellow (**4**–**6**) air-stable solids in 71–94% yields (see Scheme S1 and experimental details in the Supporting Information).

Regarding the last synthetic step, the cyclization reaction, we first investigated the ring closure of compound 1-(2-diphenylphosphinophenyl)-naphthalene (**1a**, Scheme 3),[23] which possesses a central core without methyl substituent as in **1** (Scheme S1). The reaction of **1a** with copper(II) triflate yielded two products in 30:70 ratio according to the ^{31}P NMR spectrum of the reaction mixture, which revealed two major signals at 23.8 and 4.4 ppm (Figure S1, Supporting Information). Based on the chemical shift, the main component with high field resonance is ascribed to the constitutional isomer with a six-membered ring, whereas the low-field singlet presumably corresponds to the phosphole-type heterocyclic salt (Scheme 3), for which the ^{31}P signals are typically found around 20–30 ppm in related hydrocarbon backbones.[8a,10,20a,24] In addition, the mass spectrum of the mixture shows a single peak at m/z = 387.13, which matches the molecular mass of both proposed isomeric products. Unfortunately, it was virtually impossible to separate these products by column chromatography or crystallization. The ratio of five- and six-membered cycles is nearly independent from the cyclization conditions, such as temperature, concentration, or the nature of Cu^{II} salt. To exclude the formation of phosphole-based isomers, the methyl-substituted naphthalene and phenanthrene cores (Scheme 1 and Scheme S1 in the Supporting Information) were employed for the selective preparation of **1c** and **2c**.

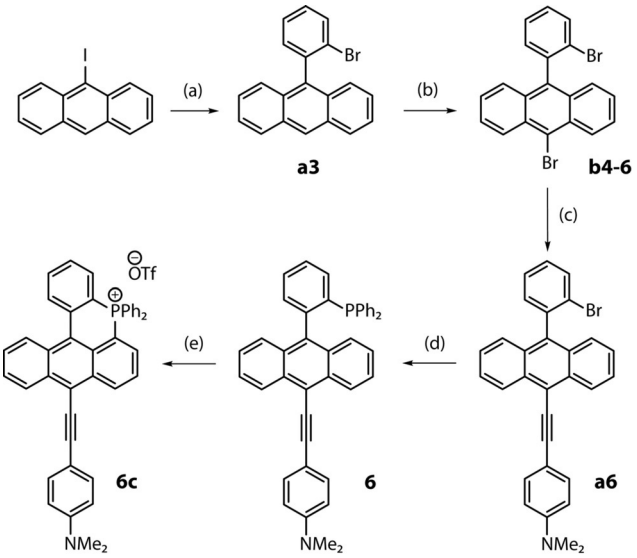

Scheme 2. Reaction pathway to phosphaannulated salt **6c**: (a) *o*-$BrC_6H_4B(OH)_2$, K_2CO_3, $Pd(PPh_3)_2Cl_2$, 1,4-dioxane/H_2O, 90 °C, 3 h, 72%;. (b) NBS, $CHCl_3$, RT, 12 h, 75%; (c) *p*-$HC_2C_6H_4NMe_2$, $Pd(PPh_3)_2Cl_2$, PPh_3, CuI, *i*Pr_2NH/THF (2:1), 50 °C, 10 h, 67%; (d) i) *t*BuLi 1.7 M, THF, −78 °C, 40 min; ii) PPh_2Cl, −78 °C→RT, 1 h, 78%; (e) $Cu(OTf)_2$ (anhyd) CH_2Cl_2/MeCN (2:1), RT, 10 min, 30%.

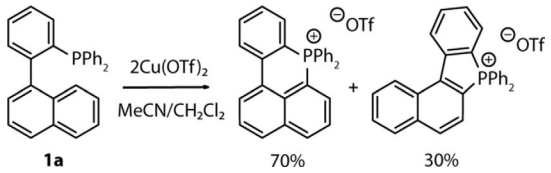

Scheme 3. Formation of five- and six-membered constitutional isomers.

We further investigated the efficiency of cyclization reaction for the synthesis of anthracene-based phosphacycle **3c** employing different copper(II) salts (Table 1). Anhydrous copper dibromide and copper acetate monohydrate in both dichloromethane/methanol and dichloromethane/acetonitrile mixtures very inefficiently promoted cyclization of the phosphine **3** as

Table 1. Cyclization of **3** mediated by Cu^{II} salts at 298 K.

Salt[a]	Solvents	Yield of **3c** [%][b]
$CuCl_2 \cdot 2H_2O$	CH_2Cl_2/MeOH 1:1	48
$Cu(ClO_4)_2 \cdot 6H_2O$	CH_2Cl_2/MeOH 1:1	25
$Cu(OTf)_2$ (anhyd)	CH_2Cl_2/MeCN 1:1	79
$CuBr_2$ (anhyd)	CH_2Cl_2/MeOH 1:1	–[c]
$Cu\ Br_2$ (anhyd)	CH_2Cl_2/MeCN 1:1	–[c]
$Cu(OAc)_2 \cdot H_2O$	CH_2Cl_2/MeOH 1:1	–[c]
$Cu(OAc)_2 \cdot H_2O$	CH_2Cl_2/MeCN 1:1	–[c]
$Cu(OTf)_2$ (anhyd) + TEMPO (5 equiv)	CH_2Cl_2/MeCN 1:1	–[c]

[a] 2.05 equiv of Cu salt. [b] Isolated yield. [c] The product was observed in trace amounts.

only trace amounts of **3c** were detected by ^{31}P NMR spectroscopy. The copper(II) chloride dihydrate, the use of which we have recently communicated,[20b] and perchlorate hexahydrate demonstrated visibly better activity, giving the isolated yields of the phosphaannulation process of 48 and 25%, respectively. The highest conversion (79%) was achieved in the case of anhydrous copper(II) triflate; therefore the latter oxidant was used for all preparations of **1c**–**6c** described in this work. This reflects a non-innocent effect of the counterions, which primarily determine the solubility of the copper salts (the least active bromide and acetate show the lowest solubility), and conceivably the degree of dissociation that evidently impacts their oxidative ability.

The cyclization reaction mediated by $Cu(OTf)_2$ gives phosphonium salts **1c**–**4c** in good yields (62–79% after chromatographic purification). However, the yields for dyes **5c** and **6c** were substantially decreased (38 and 30%), which might be explained by their lower stability on silica gel. Compounds **1c**–**4c** have a comparable solubility in aqueous media (about 0.05–0.3 mg mL^{-1} at 298 K), whereas **5c** and **6c** with extended hydrocarbon systems are relatively more hydrophobic.

The analysis of the previously reported metal-mediated phosphacyclization reactions, which involve Au^I,[24–25] Ag^I,[26] Mn^{III},[26a] and Cu^{II}[20a,27] species, allows us to assume a plausible reaction pathway presented in Scheme 4. Firstly, phosphoniumyl radical cation[28] presumably forms from the parent phosphine in the presence of copper(II) triflate by means of a single-electron transfer (SET). In the next step, the highly reactive electrophilic P-cation produces the annulated radical intermediate through P–C_{PAH} bond formation (PAH = polycyclic aromatic hydrocarbon). This is followed by the oxidation of the cyclic intermediate with a second equivalent of Cu^{II} ions and proton elimination to give the resultant phosphonium heterocycle. The involvement of radical species in the key stages of the hypothesized process is confirmed by the experiment carried out in the presence of 2,2,6,6-tetramethylpiperidine *N*-oxide (TEMPO), a widely used radical scavenger.[29] The addition of TEMPO to the starting phosphine **3** prior to the treatment with $Cu(OTf)_2$ completely suppresses the cyclization reaction (Table 1, last entry).

High-resolution ESI^+ mass spectra of annulated compounds **1c**–**6c** displayed the signals of the mono cations with m/z = 401.1, 451.2, 437.1, 513.2, 680.3 and 580.2 (Figure S2, Supporting Information), in agreement with the expected formulae. The ^{31}P NMR spectra of **1c**–**6c** showed in turn a singlet resonance, which is consistent with a same stereochemistry for all -PPh_2^{cyclo+}- fragments, with similar chemical shifts (δ = 4.4–5.7 ppm, Figure S1 in the Supporting Information).

Molecular structures of **1c**, **2c** and **4c** determined by single-crystal X-ray diffraction analysis are shown in Figures 3 and S3; the relevant data are given in Tables S1 and S2 (Supporting Information). In contrast with previously reported fused six-membered P-heterocycles,[19] the phosphorus centers are slightly out-of-plane with one phenyl ring being nearly perpendicular to the main scaffold. In compounds **1c**, **2c** and **4c**, the heteroatom adopts a somehow distorted tetrahedral geometry; the C-P-C angles are close to the idealized value of 109.5° (Table S2, Supporting Information), although larger deviations are found inside the P-cycles [103.4(2)-105.1(6)°] indicating certain geometric strain. The hydrocarbon backbones in **1c**, **2c**, and **4c** are visibly twisted due to intramolecular steric repulsion; the dihedral angles between the corresponding C_6H_4 and PAH planes are 27.0 (**1c**), 32.3 (**2c**), and 37.1° (**4c**).

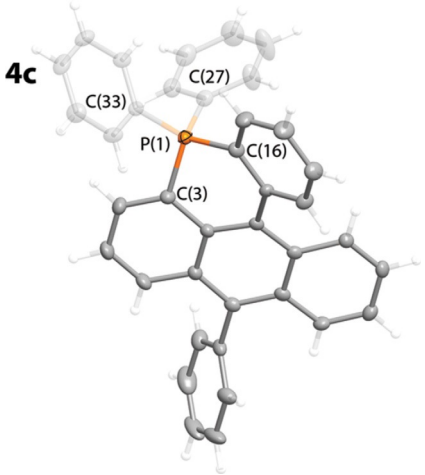

Figure 3. Molecular view of phosphacycle **4c**. Thermal ellipsoids are shown at the 50% probability level. Triflate counterion is omitted for clarity.

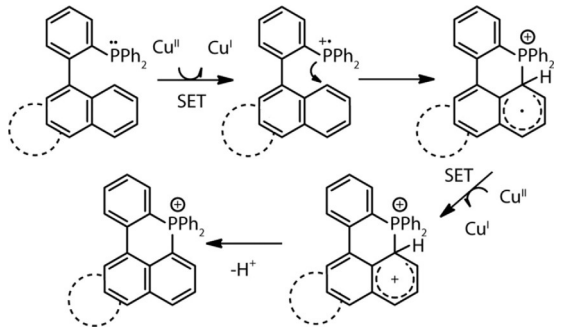

Scheme 4. Proposed mechanism for the phosphaannulation reaction.

Because of this distortion, phosphacyclic motifs feature a boat-like conformation, which is reminiscent to the configuration of a family of acridophosphine compounds,[30] but it is not observed in the planar systems based on the naphthalene moiety.[19a,25,27] The C–P bond lengths in **1c**, **2c**, and **4c** are in the range 1.765(2)–1.796(1) Å; the observed parameters are typical for P heterocyclic compounds with λ^5-σ^4 or λ^4-σ^4 phosphorus centers, such as phosphole oxides,[7c,31] phospha-fluorescein,[15] and related derivatives including cyclic phosphonium salts.[30]

In the crystals, cations **1c**, **2c**, and **4c** are arranged in a "head-to-tail" fashion, forming the dimer pairs due to π–π stacking interactions between their polyaromatic cores (Figure S3, Supporting Information). In addition to the π-interactions, the arrangement of **1c**, **2c**, and **4c** in the solid state is stabilized by the extensive hydrogen bonding, S=O···H–C [2.439(5)–2.67(1) Å], which involves triflate counterions (Figure S3, Supporting Information).

Theoretical calculations and optoelectronic properties

First insights into the optoelectronic properties of compounds **1c**–**6c** came from DFT calculations at the B3LYP/6–311+G(d) level of theory (see Supporting Information for details). Optimized geometries and molecular orbital levels are given in Figures S4–S6 and Table S3 (Supporting Information).

Regarding the structural characteristics, the results of computational studies match the experimental observations obtained from X-ray analyses. Supporting our strategy to obtain organophosphorus NIR dyes, compounds **1c**–**6c** clearly demonstrate decreasing optical band gaps (Figure S7 and Table S3, Supporting Information). Although different methods were utilized for the DFT calculations, the frontier orbital energies of **1c** (−2.559 eV for LUMO and −6.534 eV for HOMO) significantly differ from the ones of the phosphaphenalene oxide congener (−2.165 eV for LUMO and −6.162 eV for HOMO).[19b] This indicates that the introduction of a quaternized phosphorus atom into a fused P-heterocyclic systems substantially reduces both the LUMO and HOMO energies compared with the $\lambda^5\sigma^4$ oxide analogue.

Extending the π-conjugation of the polyaromatic core from naphthalene to phenanthrene (**2c**) and anthracene (**3c**) results in a more pronounced decrease of the optical band gap from 3.975 eV for **1c** to 3.03 eV for **3c** due to stabilization of LUMO and destabilization of HOMO (Figure S7, Supporting Information). Thus, within the selected PAH fragments, anthracene appears to be the most suitable block to obtain narrow-bandgap molecules by the construction of D–A systems on its basis. Indeed, DFT calculations confirmed that tailoring electron donating substituents to **3c**, namely phenyl (**4c**), *p*-(diphenylamino)phenylene (**5c**) and 4-(*N*,*N*-dimethyl)-phenylethynyl (**6c**), decreased the HOMO–LUMO gap in the order **4c**>**5c**>**6c**. This strategy afforded a prominent reduction of the optical band gap of 1.76 eV, from 3.975 eV (**1c**) to 2.215 eV for **6c** (see Table S3 in the Supporting Information).

To provide experimental insight into the electronic properties of the cationic phosphacycles, we performed electrochemical measurements of the representatively chosen naphthalene (**1c**) and anthracene (**3c**) derivatives, and the extended D–A system **6c**. The voltammograms obtained by cyclic, differential pulse and square wave voltammetry measurements (Figure S8 and Table S5 in the Supporting Information) reveal three reduction processes at −1.27, −1.66, and −1.89 V for **1c**. Dye **3c** with a higher calculated HOMO energy, shows an oxidation peak at +1.64 V in addition to reduction waves at −0.87 and −1.92 V. Likewise, **6c** exhibits lower oxidation and reduction potentials at +0.96 V, and −0.79, −1.25, and −1.95 V, respectively, as a reflection of its smaller estimated bandgap.

To complement the information obtained by theoretical calculations and electrochemical measurements, we investigated the steady-state photophysical properties of compounds **1c**–**7c**. Optical behavior of the diphosphonium salt **7c**[27] has not been investigated previously and therefore we included this compound in the current work (Figure 4). The pertinent photophysical data for the phosphacycles **1c**–**7c** in solution are summarized in Table 2 and depicted in Figures 5 and 6, and Figures S9 and S10 in the Supporting Information. The electronic absorption spectra of compounds **1c**–**4c** and **7c** recorded for water solutions ($c=10^{-5}$ M) reveal high energy (HE) bands in the range of 260–275 nm with molar extinction coefficients (ε) varying from 5900 to 37600 $M^{-1}cm^{-1}$; the largest values belong to anthracene derivatives **3c** and **4c** (Figure 5).

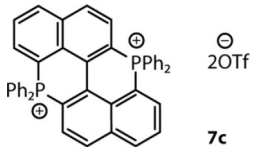

Figure 4. Structure of the binaphthyl-dicyclophosphonium salt **7c** first prepared by Nieto et al.[27]

These intense absorptions can be correlated with mixed transitions that involve orbitals from HOMO-2 to LUMO+2 (Tables S3 and S4, Supporting Information), although HE transitions evaluated by TD-DFT calculations at the B3LYP/6–311+G(d) level of theory by using the PCM model and water as solvent are systematically underestimated and differ for approximately 100 nm from the observed values (see Table 2 and Table S4 in the Supporting Information). In turn, the lower energy (LE) bands are progressively redshifted in the order **1c** (348 nm, naphthalene) ≤ **2c** (344, 375 nm, phenanthrene) < **3c** (438 nm, anthracene) < **4c** (450 nm, phenylanthracene), which is in line with the extension of π-conjugated motifs. LE absorptions possess no vibronic bands and exhibit moderate molar absorptivity ($\varepsilon \approx 6700$–10800 $M^{-1}cm^{-1}$). The predicted LE transitions also appear at lower energies but clearly reproduce this trend and can be mostly attributed to HOMO–LUMO transitions (Table S4, Supporting Information), which occur predominantly within the PAH fragment and the connecting phenylene ring (Figures S4 and S5, Supporting Information). In contrast to **1c**–**4c**, compound **7c**, which features a nearly planar binaphthyl skeleton fused with two phosphacycles, displays LE bands ($\lambda_{abs}=370$–415 nm) with a clear vibronic progression ($\Delta\nu$ = ca. 1340–1440 cm^{-1}, Figure 5). This is tentatively attributed to a more rigid and symmetrical scaffold.

Compounds **5c** and **6c** are more hydrophobic than their congeners **1c**–**4c**, **7c** and are only sparingly soluble in water.

Table 2. Photophysical properties of **1c–7c** in solution at 298 K.

	λ_{abs} [nm] (ε in 10^3 M^{-1} cm^{-1})	λ_{em} [nm]	$\Delta\nu$ [cm^{-1}]	τ [ns][a]	Φ_{em}[b]	δ_2 [GM][c]
1c[d]	275 sh (5.9), 344 (7.0)	420	5260	3.3	0.38	277 ± 24
1c[e]	277 sh (5.4), 338 sh (5.0), 352 (6.2)	418	4405	2.4	0.30	–
2c[d]	268 (21.7), 290 (12.3), 344 (11.2), 375 (5.1)	425	3137	3.5	0.49	183 ± 16
3c[d]	272 (37.6), 360 (1.1), 379 (2.3), 438 (6.7)	533	4070	16.0	0.99	637 ± 43
3c[e]	275 (39.1), 362 (1.2), 380 (2.2), 445 (6.8), 470 sh (6.2)	519	3104	14.0	0.69	–
4c[d]	274 (35.8), 362 (0.7), 383 (1.8), 450 (9.1)	547	3941	9.3	0.69	634 ± 37
5c[f]	281 (31.2), 472 (7.1)	640	5561	3.5	≈0.02	151 ± 10[g]
5c[e]	280 (38.0), 307 sh (24.5), 480 (7.9)	760	7676	3.4	0.10	–
5c[h]	280 (29.5), 472 (6.9)	640	5561	3.3	≈0.02	–
6c[f]	277 (28.3), 365 (7.9), 540 (14.5)	665	3481	–[i]	≈0.01	266 ± 18[g]
6c[e]	276 (27.6), 367 (8.5), 570 (17.4)	780	4723	1.5	0.18	–
6c[h]	272 (32.3), 374 (7.2), 555 (10.3)	690	3526	–[i]	≈0.01	–
7c[d]	260 (26.2), 330 (6.4), 372 sh (5.5), 393 (10.5), 415 (10.8)	453	2021	0.9	0.11	708 ± 34

[a] The main component of the fluorescence lifetime. [b] Relative to coumarin 480 dye (Φ_{em} = 0.87) in MeOH for **1c–2c** and **7c**, to DCM dye (Φ_{em} = 0.44) in MeOH for **3c–6c**, to LDS821 dye (Φ_{em} = 0.11) in CH_2Cl_2 for **5c–6c**. [c] Averaged value of three replicas measured by using the *Z*-scan method at 800 nm (GM = 1×10^{-50} cm^4 s photon^{-1} molecule^{-1}). [d] In H_2O (1×10^{-5} M solution). [e] In CH_2Cl_2 (1×10^{-5} M solution). [f] In H_2O with 5% of DMSO (1×10^{-5} M solution). [g] Measured in MeOH. [h] In phosphate buffered saline (PBS) with 5% of DMSO (1×10^{-5} M solution). [i] Could not be accurately determined.

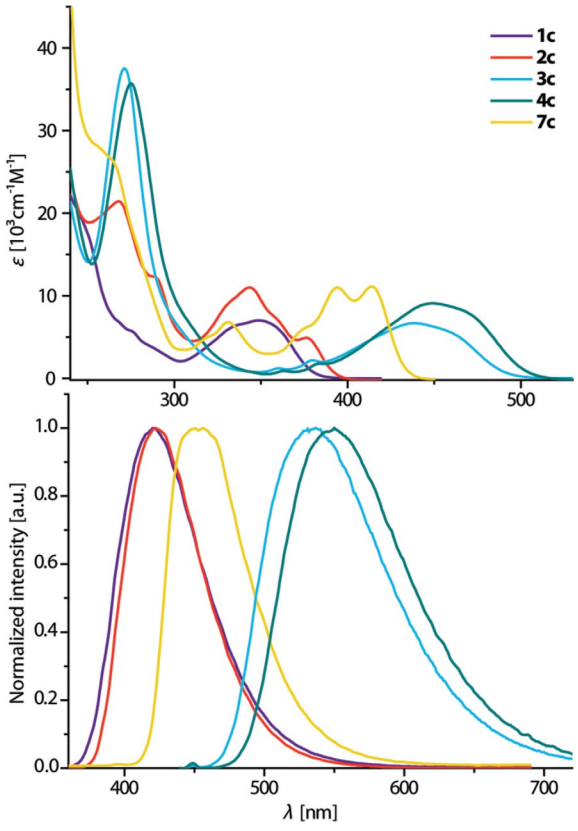

Figure 5. UV/Vis absorption (top) and normalized emission (bottom) spectra of phosphacycles **1c–4c** and **7c** (H_2O, 298 K).

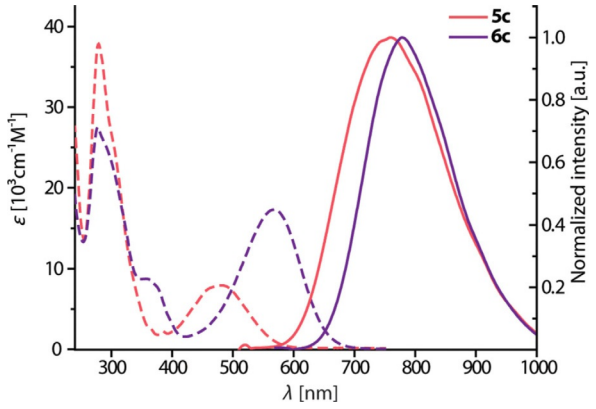

Figure 6. UV/Vis absorption (dashed lines) and normalized emission (solid lines) spectra of phosphacycles **5c** and **6c** (CH_2Cl_2, 298 K).

Therefore, the optical properties of **5c** and **6c** were studied in water and phosphate buffered saline (PBS) solutions containing 5% of dimethyl sulfoxide (DMSO), as well as in dichloromethane (Figure 6 and Figures S9 and S10 in the Supporting Information). The absorption profiles for **5c** and **6c** resemble in general those of **3c**, **4c** and reveal very similar HE bands around 270–280 nm, which are rather insensitive to the nature of the solvents (Figure S9, Supporting Information). The broad LE maxima for **5c** and **6c** are redshifted with respect to compounds **1c–4c** and **7c**, apparently due to a greater charge transfer character of the HOMO→LUMO transitions, caused by a donor–acceptor nature of the former dyes as confirmed by the TD-DFT calculations (see Figure S6 in the Supporting Information). It should be mentioned that, although changes of solvent have a minor impact on the absorption features of **5c** (Table 2 and Figure S9 in the Supporting Information), **6c** exhibits a stronger dependence on the nature of the medium. The LE absorption maxima and molar extinction coefficients for **6c** are 540 nm and 14500 M^{-1} cm^{-1} in H_2O/DMSO, and 570 nm and 17400 M^{-1} cm^{-1} in CH_2Cl_2, meaning that polar protic solvents stabilize the ground state of **6c**.

As a result of the systematic extension of the π-conjugation in combination with an increasing D–A character, phosphacycles **1c–7c** exhibited fluorescence covering a wide spectral

range from blue to the near-IR region; that is, from 420 to 780 nm (Figure 5 and 6, and Figure S10 in the Supporting Information). The emission peak wavelengths follow the same trend observed for the LE bands of the absorption spectra. The naphthalene-derived cation **1c** displays deep-blue fluorescence in water ($\lambda_{em}=420$ nm) with a quite high quantum yield ($\Phi_{em}=0.38$). In dichloromethane solution, the emission maximum is found at 418 nm with a Φ_{em} of 0.30. Compared to its P-oxide congener ($\lambda_{em}=389$, $\Phi_{em}=0.14$ in CH_2Cl_2),[19b] the luminescence of the phosphonium salt **1c** shows two-fold higher Φ_{em} (in CH_2Cl_2) together with a noticeable bathochromic shift. The latter is presumably attributed to a larger delocalization of the frontier orbitals over the PR_4^+ versus PR_3=O group. Likewise, phenanthrene-based cation **2c** exhibits an additional decrease of the emission energy in water ($\lambda_{em}=425$ nm, $\Phi_{em}=0.49$) that is in line with calculated changes of the HOMO–LUMO gap (Figure S4, Supporting Information). The presence of a larger π-framework in dication **7c** causes further redshift of the emission maximum with respect to **1c** ($\Delta\nu=1734$ cm^{-1}), whereas the rigid, symmetric structure possessing two phosphonium heterocycles leads to a decrease of the Stokes shift ($\Delta\nu=2021$ cm^{-1}). The decrease of the quantum yield of **7c** ($\Phi_{em}=0.11$) relatively to **1c** might be associated with the appearance of supplementary radiationless relaxation pathways, probably due to the presence of two positively charged centers.

The photophysical properties of the anthracene-derived dyes **3c**–**6c** can be efficiently tuned by modifying the π-system of the PAH framework and further by tailoring the electronically rich ancillary groups (Figures 5 and 6, and Figure S10 in the Supporting Information). Remarkably, interchanging the main scaffold of the phosphacycles from naphthalene/phenanthrene (**1c**, **2c**) to anthracene (**3c**) leads to a significant redshift of the emission in water of up to 5047 cm^{-1} (113 nm), leading to green fluorescence ($\lambda_{em}=533$ nm) with an outstanding Φ_{em} as high as 0.99 and a long lifetime of 16 ns. This is similar to the characteristics of $\mathbf{P_cPO}$ and $\mathbf{P_cP^+}$[20b] ($\lambda_{em}=$ 536 nm and 527 nm, $\Phi_{em}\approx1$, Figure S11 in the Supporting Information), which contain strong electron-accepting groups [-P(O)Ph_2, -P^+Ph_2] in the *ortho*-position of phenylene rings appended to the anthracene motifs. Furthermore, the presence of an unsubstituted phenyl ring attached to the acene system in dye **4c** causes some reduction of the emission energy versus **3c** ($\Delta\nu=480$ cm^{-1} or ≈14 nm) and a decrease of the fluorescence quantum yield to 0.69. This drop in efficiency can be ascribed to an increase of the degrees of freedom associated with the inclusion of a pendant phenyl ring into the anthracene moiety (Scheme 1 and Scheme S11 in the Supporting Information). An analogous influence was reported in other fluorescent molecules.[32]

Compounds **5c** and **6c** emit in the NIR region; their luminescence properties are strongly influenced by the greater donor–acceptor character. In water/DMSO and PBS/DMSO solutions **5c** with a -NPh_2 electron-rich fragment displays a broad emission band at 640 nm although at a rather low Φ_{em} of 0.02. This observation is consistent with the presence of intramolecular charge transfer (ICT), which is also supported by the DFT studies (Figure S6, Supporting Information).[14,32b] In line with solvatochromism detected in the absorption spectra of **6c**, its emission is more sensitive to changes of the solvent than for **5c**. Thus, in water/DMSO mixture, **6c** exhibits a band maximized around 665 nm that is redshifted in a more ionic PBS/DMSO solution to about 690 nm (Figure S10 in the Supporting Information). The decrease of the emission energy for **6c** versus **5c** arises from both the stronger electron-donating properties of the -NMe_2 group versus -NPh_2, and the extension of the π-conjugation through the ethynyl spacer.

Compared to the aqueous media, the photoluminescence bands of **5c** and **6c** in dichloromethane appear in a region of substantially lower energies and are accompanied by relatively higher quantum yields, that is, $\lambda_{em}=760$ nm, $\Phi_{em}=0.1$ for **5c**, and $\lambda_{em}=780$ nm, $\Phi_{em}=0.18$ for **6c**. Considering that CH_2Cl_2 has a lower polarity than water, **5c** and **6c** show negative solvatochromism (both in absorption and emission spectra), which is not exceptional for ionic compounds with ICT behavior. This is typically explained by a decrease of the dipole moment upon excitation that leads to destabilization of the relaxed S_1 state in a more polar solvent.[33]

With respect to the predecessor **1c**, the performed changes of the molecular structure resulted in a remarkable 12103 cm^1 (362 nm) bathochromic shift of fluorescence demonstrated by **6c**. It is important to note that the emission characteristics of **5c** and **6c** in organic solvents place them among the most efficient and red shifted organophosphorus dyes reported to date.[13b,14,15,16a,34] The photoinduced intramolecular charge transfer leads in turn to large Stokes shifts of approximately 7600 cm^{-1} (280 nm, **5c**) and 4700 cm^{-1} (230 nm, **6c** Figure 6), minimizing the reabsorption, which is crucial for practical imaging applications.[35]

To highlight the importance of the phosphonium group for tuning optical properties of these polyaromatic dyes, it is worth comparing **1c**–**5c** (Figure S12, Supporting Information) with their reported non-phosphinated acene precursors (i.e., phenyl-naphthalene/[36] phenanthrene/[37] anthracene,[38] diphenylanthracene,[39] and its -NPh_2 derivative[40]). The experimental data confirm that the modification of the given PAH systems with the cationic group drastically decreases the emission energy. In this regard, it should be mentioned that **6c** shows a perceptibly red shifted fluorescence than linear extended donor–acceptor systems employing the same anthracene-ethynyl-dimethylaniline core.[41]

It is also worth noting that the emission spectrum of **6c** in the pristine solid exhibits an NIR emission band maximized at 825 nm (see Figure S13) with an approximately 7% emission quantum yield ($\tau_f\approx550$ ps). Due to the lack of solvent relaxation and hence solvatochromism, the further redshift of the NIR emission of **6c** in solid (cf. in solution) should originate from the solid polyaromatic packing, the topic of which is out of current focus but is worthy of pursuit in the future.

The significant delocalization of the frontier orbitals and particularly the donor–acceptor nature of compounds **1c**–**7c** motivated us to investigate their non-linear optical characteristics. Essentially, all species have an appreciable two-photon absorption (TPA) property. According to the *Z*-scan data, obtained by

using the excitation wavelength 800 nm, the corresponding cross-section δ_2 amounts to 151–708 GM (Table 2 and Figure S14 in the Supporting Information); this performance is commensurable to those of the reported TPA fluorescent dyes.[3b] The highest δ_2 value, obtained for the dicationic heterocycle **7c**, is considerably larger than those for coumarin 485/480, fluorescein, and rhodamine 6G and B dyes ($\delta_2 = 36$–160 GM at 800 nm).[42]

Furthermore, we evaluated the photostability of compounds **1c**–**7c** in solution. In general, the family of polycyclic hydrocarbons including phenanthrene and anthracene is thermally stable in the solid state, but is sensitive to oxidation by molecular O_2 to give non-emissive endoperoxides or quinone derivatives.[43] Alternatively, quaternized phosphonium cations can decompose under the basic conditions.[44] Thus, the stability of dyes **1c**–**4c** and **7c** under continuous irradiation was studied in aerated PBS solutions (optical density $A = 0.1$, pH 7.4), the hydrophobic **5c**, **6c** were investigated in aerated dichloromethane ($A = 0.1$), see Figures S15 and S16 in the Supporting Information. The phosphacycles were divided into three groups according to their fluorescence color, excitation wavelength and the reference dye: **1c** and **2c** (blue emission, $\lambda_{exc} =$ 375 nm, coumarin 480); **3c**, **4c** and **7c** (green-blue emission, $\lambda_{exc} = 458$ nm, coumarin 480, and fluorescein); **5c** and **6c** (red emission, $\lambda_{exc} = 532$ nm, LDS821). The change of the fluorescence intensity (I/I_o) at the emission maxima was monitored for 30 min and revealed that compounds **1c**, **5c**, **6c** and **7c** demonstrated visibly smaller photodegradation than their commercial counterparts coumarin 480, LDS821, and fluorescein, respectively, whereas **3c** and **4c** showing the I/I_o ratio approximately 92% were only slightly less stable than fluorescein ($I/I_o \approx 96\%$, Figure S16 in the Supporting Information).

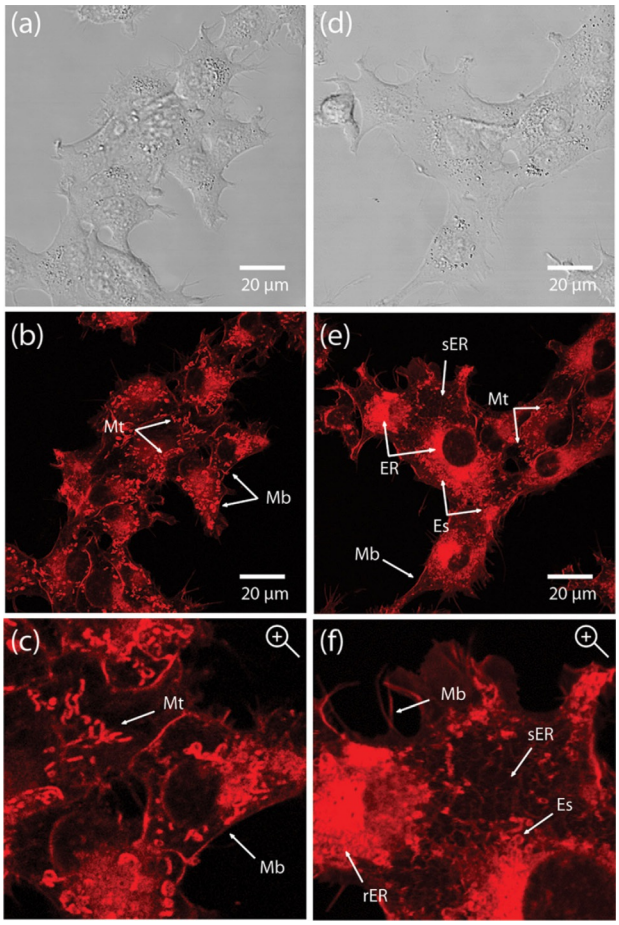

Figure 7. Confocal images of living HeLa cells labeled with compound **6c**. (a, d) Bright-field images, (b, e) two-photon fluorescence images ($\lambda_{ex} = 800$ nm), and (c, f) zoom-in images of (b) and (e). Cells co-cultured with **6c** for 10 min and for 2 hours were shown in the first (a–c) and second column (d–f), respectively. Mt: mitochondria, Mb: membrane, ER: endoplasmic reticulum, rER: rough ER, sER: smooth ER, and Es: endosome.

Bioimaging studies

In view of the good photostability and ionic nature of the titled compounds, we tested their applicability as cell imaging probes. Notably, cationic phosphonium species are known for their particular ability to penetrate through the cell membrane and localize in mitochondria,[45] which we have also demonstrated for the relevant phosphacyclic compounds.[20b] Among the studied dyes only salts **4c** and **6c** easily enter the HeLa cells within an incubation period of 1 h and, therefore, were used for staining experiments. The given cell line tolerates the concentrations of **4c** and **6c** up to 3–5 μM with negligibly small death rate (Figure S17, Supporting Information) that confirms low cytotoxicity of these fluorophores. The confocal microscopy studies of the HeLa cells, treated with **4c** (2 μM) at 37 °C, indicate that the dye is primarily accumulated in mitochondria (Figure S18, Supporting Information) and demonstrates strong emission upon one-photon excitation ($\lambda_{ex} =$ 405 nm, blue channel). Figures 7 and Figure S19 (Supporting Information) show the confocal images of living HeLa cells labeled with compound **6c**, taken in different time periods. For this dye, we have also followed the progression of labeling within a minute (Figure S20, Supporting Information). The probe **6c** was mixed with preheated Dulbecco's modified eagle medium (DMEM; 37 °C) and was gently added to the cells. Owning to the hydrophobicity of **6c**, it tended to accumulate on phospholipid-rich cell membrane at the beginning. As time progresses, other organelles containing lipid bilayer, such as mitochondria, rough and smooth endoplasmic reticulum (ER) were also labeled. The individual and fused mitochondria were observed as well. The magnified images shown in Figures 7c,f and Figure S21 (Supporting Information) revealed the morphodynamic changes of fused mitochondria. Similarly, lipid-rich ERs, including smooth ER (sER) and rough ER (rER), were stained.

The sERs dispersed in cytosol as fiber-like network, whereas most of the rERs were gathered around the nuclei. We further studied the physiological status of cells incubated with **6c**. Following the same protocol of treatment, the probes were mainly found in fused mitochondria in healthy cells. In contrast, considerable vacuoles were observed in 3-day-growth cells cultured in unreplaced DMEM. The great number of vacuoles indicated that cells were unhealthy and tended to accumulate waste products (Figure S22, Supporting Information). Interestingly, as the old DMEM was replaced with fresh one,

the formation of endocytic vesicles appeared near the cell membrane. These results clearly indicate that **6c** is advantageous for studies of membrane dynamics, endocytosis, exocytosis, and organelles interaction.

Conclusions

A facile method of intramolecular phosphacyclization, which results in quaternization of a trivalent phosphorus center in the presence of Cu^{II} salts through P–C bond formation, has been successfully applied to the series of rationally designed tertiary phosphines containing polyaromatic fragments. Following this approach, we synthesized a family of new organophosphorus cationic fluorophores, which comprise six-membered P-heterocycle fused with PAH moieties. Changing the hydrocarbon core from naphthalene (**1c**) to anthracene (**3c**) caused a substantial bathochromic shift of the emission from 420 to 530 nm (in water) and simultaneously provided extremely high quantum yield near unity. The subsequent decrease of the HOMO–LUMO gap was achieved by constructing donor–acceptor architectures on the basis of the anthracene framework. Appending electron-rich substituents to this polycyclic scaffold, which incorporates electron withdrawing phosphonium group, produced molecular systems **5c** and **6c** exhibiting low energy intramolecular charge transfer. As a consequence, these dyes showed dramatically reduced bandgap that led to near-IR fluorescence with good quantum efficiency ($\lambda_{em}=780$ nm, $\Phi_{em}=0.18$ for **6c** in dichloromethane) and large Stokes shifts reaching the value of 7600 cm^{-1} (280 nm for **5c**). This photophysical performance, along with their low toxicity, high photostability and decent two-photon absorption properties, allowed for probing the title dyes for cell staining. Although in aqueous polar media the emissions of both **5c** and **6c** were hypsochromically shifted, the results of imaging experiments confirm the applicability of these dyes for visualization of the biological objects. In a broader view, a particularly wide tunability of the optical behavior, demonstrated within the given family of polycyclic phosphonium fluorophores, points to a promising potential of the presented molecular design for the engineering of dyes with diverse photophysical functionalities.

Experimental Section

Crystallographic data

CCDC 1876636 (**1c**), 1876637 (**2c**), and 1876638 (**4c**) contain the supplementary crystallographic data for this paper. These data are provided free of charge by The Cambridge Crystallographic Data Centre.

Acknowledgements

P.H. thanks the Hanns-Seidel-Stiftung for a fellowship. C.R.N acknowledges the financial support from projects RO4899/4-1 and SBPLY/17/180501/000518. I.O.K. thanks Academy of Finland (grant 317903). A.B. acknowledges the financial support from the Saastamoinen Foundation.

Conflict of interest

The authors declare no conflict of interest.

Keywords: cyclization · dyes · imaging · optoelectronic properties · phosphorus heterocycles

[1] a) H. Dong, H. Zhu, Q. Meng, X. Gong, W. Hu, *Chem. Soc. Rev.* **2012**, *41*, 1754 – 1808; b) X. Yang, X. Xu, G. Zhou, *J. Mater. Chem. C* **2015**, *3*, 913 – 944; c) Y. Im, M. Kim, Y. J. Cho, J.-A. Seo, K. S. Yook, J. Y. Lee, *Chem. Mater.* **2017**, *29*, 1946 – 1963.

[2] a) X. Li, X. Gao, W. Shi, H. Ma, *Chem. Rev.* **2014**, *114*, 590 – 659; b) S. Shanmugaraju, P. S. Mukherjee, *Chem. Commun.* **2015**, *51*, 16014 – 16032; c) Z. Xu, L. Xu, *Chem. Commun.* **2016**, *52*, 1094 – 1119; d) D. Andina, J.-C. Leroux, P. Luciani, *Chem. Eur. J.* **2017**, *23*, 13549 – 13573.

[3] a) H. Kobayashi, M. Ogawa, R. Alford, P. L. Choyke, Y. Urano, *Chem. Rev.* **2010**, *110*, 2620 – 2640; b) H. M. Kim, B. R. Cho, *Chem. Rev.* **2015**, *115*, 5014 – 5055; c) H. Zhu, J. Fan, J. Du, X. Peng, *Acc. Chem. Res.* **2016**, *49*, 2115 – 2126.

[4] a) T. Baumgartner, *Acc. Chem. Res.* **2014**, *47*, 1613 – 1622; b) D. Joly, P.-A. Bouit, M. Hissler, *J. Mater. Chem. C* **2016**, *4*, 3686 – 3698; c) M. A. Shameem, A. Orthaber, *Chem. Eur. J.* **2016**, *22*, 10718 – 10735; d) R. Szűcs, P.-A. Bouit, L. Nyulászi, M. Hissler, *ChemPhysChem* **2017**, *18*, 2618 – 2630; e) M. Stolar, T. Baumgartner, *Chem. Commun.* **2018**, *54*, 3311 – 3322; f) E. Regulska, C. Romero-Nieto, *Dalton Trans.* **2018**, *47*, 10344 – 10359.

[5] a) Y. Ren, T. Baumgartner, *Dalton Trans.* **2012**, *41*, 7792 – 7800; b) P.-A. Bouit, A. Escande, R. Szűcs, D. Szieberth, C. Lescop, L. Nyulászi, M. Hissler, R. Réau, *J. Am. Chem. Soc.* **2012**, *134*, 6524 – 6527; c) Z. Wang, B. S. Gelfand, T. Baumgartner, *Angew. Chem. Int. Ed.* **2016**, *55*, 3481 – 3485; *Angew. Chem.* **2016**, *128*, 3542 – 3546; d) R. A. Adler, C. Wang, A. Fukazawa, S. Yamaguchi, *Inorg. Chem.* **2017**, *56*, 8718 – 8725.

[6] a) O. Fadhel, M. Gras, N. Lemaitre, V. Deborde, M. Hissler, B. Geffroy, R. Réau, *Adv. Mater.* **2009**, *21*, 1261 – 1265; b) F. Riobé, R. Szűcs, P.-A. Bouit, D. Tondelier, B. Geffroy, F. Aparicio, J. Buendía, L. Sánchez, R. Réau, L. Nyulászi, M. Hissler, *Chem. Eur. J.* **2015**, *21*, 6547 – 6556.

[7] a) C. Reus, T. Baumgartner, *Dalton Trans.* **2016**, *45*, 1850 – 1855; b) N. M.-W. Wu, M. Ng, W. H. Lam, H.-L. Wong, V. W.-W. Yam, *J. Am. Chem. Soc.* **2017**, *139*, 15142 – 15150; c) N. M.-W. Wu, H.-L. Wong, V. W.-W. Yam, *Chem. Sci.* **2017**, *8*, 1309 – 1315.

[8] a) E. Yamaguchi, C. Wang, A. Fukazawa, M. Taki, Y. Sato, T. Sasaki, M. Ueda, N. Sasaki, T. Higashiyama, S. Yamaguchi, *Angew. Chem. Int. Ed.* **2015**, *54*, 4539 – 4543; *Angew. Chem.* **2015**, *127*, 4622 – 4626; b) M. Taki, H. Ogasawara, H. Osaki, A. Fukazawa, Y. Sato, K. Ogasawara, T. Higashiyama, S. Yamaguchi, *Chem. Commun.* **2015**, *51*, 11880 – 11883.

[9] Y. Takeda, K. Hatanaka, T. Nishida, S. Minakata, *Chem. Eur. J.* **2016**, *22*, 10360 – 10364.

[10] Y. Matano, A. Saito, T. Fukushima, Y. Tokudome, F. Suzuki, D. Sakamaki, H. Kaji, A. Ito, K. Tanaka, H. Imahori, *Angew. Chem. Int. Ed.* **2011**, *50*, 8016 – 8020; *Angew. Chem.* **2011**, *123*, 8166 – 8170.

[11] a) C. Reus, M. Stolar, J. Vanderkley, J. Nebauer, T. Baumgartner, *J. Am. Chem. Soc.* **2015**, *137*, 11710 – 11717; b) T. W. Greulich, E. Yamaguchi, C. Doerenkamp, M. Lübbesmeyer, C. G. Daniliuc, A. Fukazawa, H. Eckert, S. Yamaguchi, A. Studer, *Chem. Eur. J.* **2017**, *23*, 6029 – 6033.

[12] P. Hindenberg, C. Romero-Nieto, *Synlett* **2016**, *27*, 2293 – 2300.

[13] a) X. Chai, X. Cui, B. Wang, F. Yang, Y. Cai, Q. Wu, T. Wang, *Chem. Eur. J.* **2015**, *21*, 16754 – 16758; b) X. Zhou, R. Lai, J. R. Beck, H. Lia, C. I. Stains, *Chem. Commun.* **2016**, *52*, 12290 – 12293.

[14] M. Grzybowski, M. Taki, S. Yamaguchi, *Chem. Eur. J.* **2017**, *23*, 13028 – 13032.

[15] a) A. Fukazawa, S. Suda, M. Taki, E. Yamaguchi, M. Grzybowski, Y. Sato, T. Higashiyama, S. Yamaguchi, *Chem. Commun.* **2016**, *52*, 1120 – 1123; b) A. Fukazawa, J. Usuba, R. A. Adler, S. Yamaguchi, *Chem. Commun.* **2017**, *53*, 8565 – 8568.

[16] a) H. Ogasawara, M. Grzybowski, R. Hosokawa, Y. Sato, M. Taki, S. Yamaguchi, *Chem. Commun.* **2018**, *54*, 299 – 302; b) M. Grzybowski, M. Taki, K. Senda, Y. Sato, T. Ariyoshi, Y. Okada, R. Kawakami, T. Imamura, S. Yamaguchi, *Angew. Chem. Int. Ed.* **2018**, *57*, 10137 – 10141; *Angew. Chem.* **2018**, *130*, 10294 – 10298.

[17] N. Hashimoto, R. Umano, Y. Ochi, K. Shimahara, J. Nakamura, S. Mori, H. Ohta, Y. Watanabe, M. Hayashi, *J. Am. Chem. Soc.* **2018**, *140*, 2046 – 2049.

[18] a) T. Hatakeyama, S. Hashimoto, M. Nakamura, *Org. Lett.* **2011**, *13*, 2130 – 2133; b) S. Hashimoto, S. Nakatsuka, M. Nakamura, T. Hatakeyama, *Angew. Chem. Int. Ed.* **2014**, *53*, 14074 – 14076; *Angew. Chem.* **2014**, *126*, 14298 – 14300.

[19] a) C. Romero-Nieto, A. López-Andarias, C. Egler-Lucas, F. Gebert, J.-P. Neus, O. Pilgram, *Angew. Chem. Int. Ed.* **2015**, *54*, 15872 – 15875; *Angew. Chem.* **2015**, *127*, 16098 – 16102; b) P. Hindenberg, A. López-Andarias, F. Rominger, A. de Cózar, C. Romero-Nieto, *Chem. Eur. J.* **2017**, *23*, 13919 – 13928.

[20] a) Q. Ge, J. Zong, B. Li, B. Wang, *Org. Lett.* **2017**, *19*, 6670 – 6673; b) A. Belyaev, Y.-T. Chen, S.-H. Su, Y.-J. Tseng, A. J. Karttunen, S. P. Tunik, P.-T. Chou, I. O. Koshevoy, *Chem. Commun.* **2017**, *53*, 10954 – 10957.

[21] a) S. Huang, L. Kötzner, C. K. De, B. List, *J. Am. Chem. Soc.* **2015**, *137*, 3446 – 3449; b) S.-z. Lin, T.-p. You, *Tetrahedron* **2009**, 65, 1010 – 1016.

[22] a) M. Shao, P. Dongare, L. N. Dawe, D. W. Thompson, Y. Zhao, *Org. Lett.* **2010**, *12*, 3050 – 3053; b) A. S. Carlstroem, T. Frejd, *J. Org. Chem.* **1991**, *56*, 1289 – 1293.

[23] S. Xu, F. Haeffner, B. Li, N. Zakharov Lev, S.-Y. Liu, *Angew. Chem. Int. Ed.* **2014**, *53*, 6795 – 6799; *Angew. Chem.* **2014**, *126*, 6913 – 6917.

[24] S. Arndt, J. Borstelmann, R. Eshagh Saatlo, W. P. Antoni, F. Rominger, M. Rudolph, Q. An, Y. Vaynzof, A. S. K. Hashmi, *Chem. Eur. J.* **2018**, *24*, 7882 – 7889.

[25] H. Kawai, W. J. Wolf, A. G. DiPasquale, M. S. Winston, F. D. Toste, *J. Am. Chem. Soc.* **2016**, *138*, 587 – 593.

[26] a) Y. Unoh, K. Hirano, T. Satoh, M. Miura, *Angew. Chem. Int. Ed.* **2013**, *52*, 12975 – 12979; *Angew. Chem.* **2013**, *125*, 13213 – 13217; b) Y.-R. Chen, W.-L. Duan, *J. Am. Chem. Soc.* **2013**, *135*, 16754 – 16757.

[27] S. Nieto, P. Metola, V. M. Lynch, E. V. Anslyn, *Organometallics* **2008**, *27*, 3608 – 3610.

[28] J. P. Bullock, A. M. Bond, R. T. Boeré, T. M. Gietz, T. L. Roemmele, S. D. Seagrave, J. D. Masuda, M. Parvez, *J. Am. Chem. Soc.* **2013**, *135*, 11205 – 11215.

[29] a) A. L. J. Beckwith, V. W. Bowry, K. U. Ingold, *J. Am. Chem. Soc.* **1992**, *114*, 4983 – 4992; b) P. J. Wright, A. M. English, *J. Am. Chem. Soc.* **2003**, *125*, 8655 – 8665.

[30] T. A. Schaub, S. M. Brells, P. O. Dral, F. Hampel, H. Maid, M. Kivala, *Chem. Eur. J.* **2017**, *23*, 6988 – 6992.

[31] X. He, A. Y. Y. Woo, J. Borau-Garcia, T. Baumgartner, *Chem. Eur. J.* **2013**, *19*, 7620 – 7630.

[32] a) Y. Hong, J. W. Y. Lam, B. Z. Tang, *Chem. Soc. Rev.* **2011**, *40*, 5361 – 5388; b) J. Liu, Y.-Q. Sun, H. Zhang, H. Shi, Y. Shi, W. Guo, *ACS Appl. Mater. Interfaces* **2016**, *8*, 22953 – 22962; c) T. Ren, W. Xu, F. Jin, D. Cheng, L. Zhang, L. Yuan, X. Zhang, *Anal. Chem.* **2017**, *89*, 11427 – 11434.

[33] a) B. Carlotti, G. Consiglio, F. Elisei, C. G. Fortuna, U. Mazzucato, A. Spalletti, *J. Phys. Chem. A* **2014**, *118*, 3580 – 3592; b) B. Carlotti, A. Cesaretti, C. G. Fortuna, A. Spalletti, F. Elisei, *Phys. Chem. Chem. Phys.* **2015**, *17*, 1877 – 1882.

[34] a) C. Wang, A. Fukazawa, M. Taki, Y. Sato, T. Higashiyama, S. Yamaguchi, *Angew. Chem. Int. Ed.* **2015**, *54*, 15213 – 15217; *Angew. Chem.* **2015**, *127*, 15428 – 15432; b) A. N. Butkevich, M. V. Sednev, H. Shojaei, V. N. Belov, S. W. Hell, *Org. Lett.* **2018**, *20*, 1261 – 1264.

[35] a) H. Chen, B. Dong, Y. Tang, W. Lin, *Acc. Chem. Res.* **2017**, *50*, 1410 – 1422; b) I. Martinić, S. V. Eliseeva, S. Petoud, *J. Lumin.* **2017**, *189*, 19 – 43.

[36] J. B. Gallivan, *J. Phys. Chem.* **1969**, *73*, 3070 – 3075.

[37] A. Onkelinx, F. C. De Schryver, L. Viaene, M. Van der Auweraer, K. Iwai, M. Yamamoto, M. Ichikawa, H. Masuhara, M. Maus, W. Rettig, *J. Am. Chem. Soc.* **1996**, *118*, 2892 – 2902.

[38] N. Kitamura, E. Sakuda, Y. Iwahashi, K. Tsuge, Y. Sasaki, S. Ishizaka, *J. Photochem. Photobiol. A* **2009**, *207*, 102 – 108.

[39] C.-L. Wu, C.-H. Chang, Y.-T. Chang, C.-T. Chen, C.-T. Chen, C.-J. Su, *J. Mater. Chem. C* **2014**, *2*, 7188 – 7200.

[40] S. Tao, Y. Zhou, C.-S. Lee, S.-T. Lee, D. Huang, X. Zhang, *J. Phys. Chem. C* **2008**, *112*, 14603 – 14606.

[41] a) J.-H. Lin, A. Elangovan, T.-I. Ho, *J. Org. Chem.* **2005**, *70*, 7397 – 7407; b) C. Teng, X. Yang, C. Yang, S. Li, M. Cheng, A. Hagfeldt, L. Sun, *J. Phys. Chem. C* **2010**, *114*, 9101 – 9110; c) K. S. Kisel, T. Eskelinen, W. Zafar, A. I. Solomatina, P. Hirva, E. V. Grachova, S. P. Tunik, I. O. Koshevoy, *Inorg. Chem.* **2018**, *57*, 6349 – 6361; d) M.-C. Tsai, C.-L. Wang, C.-W. Chang, C.-W. Hsu, Y.-H. Hsiao, C.-L. Liu, C.-C. Wang, S.-Y. Lin, C.-Y. Lin, *J. Mater. Chem. A* **2018**, *6*, 1995 – 2003.

[42] a) N. S. Makarov, M. Drobizhev, A. Rebane, *Opt. Express* **2008**, *16*, 4029 – 4047; b) P.-H. Huang, J.-Y. Shen, S.-C. Pu, Y.-S. Wen, J. T. Lin, P.-T. Chou, M.-C. P. Yeh, *J. Mater. Chem.* **2006**, *16*, 850 – 857.

[43] C. K. Das, N. S. Das, *J. Chem. Technol. Biotechnol.* **1982**, *32*, 643 – 649.

[44] a) M. C. Hilton, R. D. Dolewski, A. McNally, *J. Am. Chem. Soc.* **2016**, *138*, 13806 – 13809; b) Z. Deng, J.-H. Lin, J.-C. Xiao, *Nat. Commun.* **2016**, *7*, 10337.

[45] J. Zielonka, J. Joseph, A. Sikora, M. Hardy, O. Ouari, J. Vasquez-Vivar, G. Cheng, M. Lopez, B. Kalyanaraman, *Chem. Rev.* **2017**, *117*, 10043 – 10120.

Manuscript received: January 9, 2019

Accepted manuscript online: February 21, 2019

Version of record online: March 27, 2019

